

Optimization of Enhanced Surfaces for High Flux Chip Cooling by Pool Boiling

I. Mudawar

Associate Professor
and Director.

T. M. Anderson¹

Boiling and Two-Phase Flow Laboratory,
School of Mechanical Engineering,
Purdue University,
West Lafayette, IN 47907

A high flux electronic chip was numerically and experimentally simulated to investigate pool boiling capabilities of enhanced metallic surface attachments built upon a $12.7 \times 12.7 \text{ mm}^2$ base area. It is shown how experimental nucleate boiling data for a flat chip and for chips with low-profile microstructures can be used as input boundary conditions in the numerical prediction of boiling performances of high flux, smooth and microstructured extended cylindrical surfaces. A technique for extending the applicability of the numerical results to cylindrical fin arrays is demonstrated with the aid of experimental data obtained for these surfaces. Surface enhancement resulted in chip planform heat fluxes of 105.4 and 159.3 W/cm², for saturated and 35°C subcooled FC-72, respectively.

1 Introduction

The continuing trend of increasing computer power has driven the number of logic devices etched onto an integrated circuit up at a rapid pace. The quest toward developing lower power logic devices has been overwhelmed by concurrent increases in switching speed and number of devices per unit area. Consequently, more powerful cooling technologies must be developed to help sustain the trends of increased miniaturization and computational power.

Direct liquid immersion cooling has great potential as a successor to air cooling and indirect liquid cooling technologies. Currently, several immersion-cooled computers are in operation. The Cray-2, for example, relies on a slow moving flow of a dielectric fluorocarbon liquid (FC-77) to dissipate heat by forced convection and localized boiling (Danielson et al., 1986). Because of its dielectric properties and chemical inertness, the FC family of fluorocarbons (manufactured by 3M) appears to be the obvious choice for direct immersion cooling of electronic hardware.

While direct immersion has been studied in the context of single-phase forced convection (Tuckerman and Pease, 1981; Samant and Simon, 1986; Ramadhyani and Incropera, 1987; Maddox and Mudawar, 1989; Mudawar and Maddox, 1989), falling films (Mudawar et al., 1987; Grimley et al., 1988), and flow boiling (Samant and Simon, 1986; Maddox and Mudawar, 1989; Mudawar and Maddox, 1989; McGillis et al., 1991), pool boiling remains a very attractive cooling option due to the unique attribute of passive fluid circulation. Having no mechanical pumps, pool boiling hardware are less complex, easier to seal and free of pump-induced fluid pulsation.

Compared to forced convection, pool boiling offers few options for enhancement of heat transfer. Liquid velocity in a flow channel enhances both single and two-phase convection and postpones critical heat flux (CHF) by sweeping away bubbles before they form an insulating vapor blanket. In pool boiling, however, the relatively weak liquid flow is induced only by natural convection prior to the onset of boiling and, thereafter, by buoyancy and bubble motion. Unfortunately, induced flow cannot be easily controlled, therefore, attempts at enhancing pool boiling performance are limited to variations of (1) fluid conditions, type of coolant, saturation pressure, and subcooling (Mudawar and Anderson, 1990); or (2) surface structure, either on a microscopic scale (Messina and Park, 1981; Anderson and Mudawar, 1989) or by a large increase of surface area (Marto and Lepere, 1982; Nakayama et al., 1984; Anderson and Mudawar, 1990).

The planar nature of the electronic chip lends itself to the attachment of extended surfaces to increase surface area and, therefore, the transfer rate from the chip. Several boiling fin design methods have been proposed in the past (Haley and Westwater, 1966; Cumo et al., 1968; Cash et al., 1971), but the specific requirements for electronic cooling were first addressed by Nakayama et al. (1984). Using a cylindrical fin constructed of stacked porous plates, they were able to dissipate over 110 W/cm² (based on planform area) in FC-72.

The present study is intended as a general guide to the packaging engineer in designing boiling fins for electronic cooling. This is achieved through adaptation of experimental nucleate boiling data measured for a flat chip and for low-profile microstructured chips in predicting boiling performance of smooth and microstructured extended surfaces, respectively. It is also the objective of this paper to examine means of combining several levels of surface enhancement to boost CHF above the chip fluxes predicted for future very large scale integration (VLSI) chips.

¹Former Graduate Research Assistant; current address: Data Systems Division, IBM, Poughkeepsie, NY 12602.

Contributed by the Electrical and Electronic Packaging Division for publication in the JOURNAL OF ELECTRONIC PACKAGING. Manuscript received by the EEPD May 5, 1992; revised manuscript received November 17, 1992. Associate Technical Editor: B. G. Sammakia.

2 Experimental Methods

The liquid encapsulated electronic cooling environment was simulated inside a stainless steel pressure vessel. As shown in Fig. 1, the vessel was fitted with three ports. A module housing the simulated chip was inserted through one port, while the other two ports were fitted with quartz windows, providing optical access in directions parallel and normal to the chip surface. The fluorocarbon liquid (FC-72 or FC-87) was pre-heated by an immersion heater submerged in the liquid, and protection against heat loss to the ambient was achieved by a band heater which was wrapped around the vessel. A water-cooled condenser, coiled in the upper section of the vessel, maintained saturation conditions throughout the boiling tests. During subcooled tests, the vessel was completely filled with liquid and independent control of liquid temperature and pressure required connecting the vessel to an external pressurization/expansion tank.

Figure 2 shows a sectional diagram of the test heater module. The enhanced surfaces were built upon a 4.78 mm-thick base chip having a cross-sectional area of $12.7 \times 12.7 \text{ mm}^2$. The chip was soldered to the end of a high-purity copper bar which conducted heat from a cartridge heater to the chip. The chip heat flux was determined by a linear fit to temperatures measured by four thermocouples which were inserted along the axis of the bar. The average base temperature for the enhanced surfaces was determined by extrapolating the temperature reading of a thermocouple embedded in the chip based on the measured thermal flux. Repeatability in the data was within $\pm 0.05^\circ\text{C}$ for heat fluxes smaller than 1 W/m^2 and $\pm 0.1^\circ\text{C}$ for higher fluxes. Further details on the calibration and accuracy of the heater measurements can be found in a previous article by the authors (Anderson and Mudawar, 1989). The same article details the procedure for obtaining boiling data.

Because temperature and heat flux measurements provide little insight into the growth, size and placement of active boiling patches on an enhanced surface, visual observation played a vital role in helping to understand boiling behavior. An extensive photographic library was created to document specific boiling events for later interpretation. High speed film and digital video cameras were also used to capture brief sequences of boiling, but the most useful information came from still photography. Still photography was used in every boiling experiment to capture the changing pattern of boiling with increasing heat flux. A Nikon camera was used in conjunction with a Vivitar 55 mm automacro lens and Vivitar 152 strobflash.

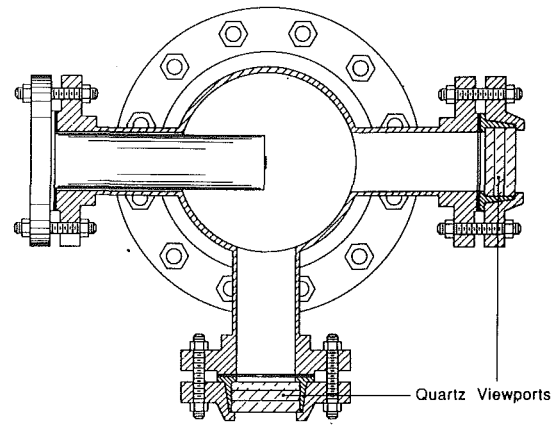


Fig. 1 Longitudinal and cross-sectional diagrams of the test chamber

Nomenclature

a = empirical constant
 A_b = base area of cylindrical fin
 A_{chip} = chip planform area ($12.7 \times 12.7 \text{ mm}^2$)
 A_e = planform area of finned element on a chip
 $A_e^+ = A_e/A_b$
 A_f = heat transfer area of cylindrical fin
 $A_f^+ = A_f/A_b$
 A_r^+ = ratio of total heat transfer area of enhanced surface to chip planform area = A_r/A_{chip}
 A_t = total heat transfer area of enhanced surface
 D = diameter of cylindrical fin
 D_b = bubble departure diameter
 g = acceleration due to gravity
 k_f = thermal conductivity of liquid

L = length of cylindrical fin
 L^+ = aspect ratio of cylindrical fin = L/D
 L_{chip} = chip length and width (12.7 mm)
 m = number of finned elements on a chip
 n = empirical constant
 \overline{Nu}_D = average Nusselt number for a horizontal cylinder of diameter $D = \frac{qD}{(\Delta T)k_f}$
 \overline{Nu}_l = average Nusselt number for a vertical plate of height $l = \frac{ql}{(\Delta T)k_f}$
 Pr_f = Prandtl number of liquid
 q = heat flux based on chip planform area A_{chip}
 q_b = heat flux of reference (flat,

microgroove or microstud) surface based on planform area
 Q_f = total heat transfer rate from cylindrical fin
 q_m = critical heat flux (CHF) based on chip planform area (A_{chip})
 $q_{m,\text{flat}}$ = critical heat flux from a vertical flat surface
 q_m^+ = normalized CHF value for enhanced surface = $\frac{q_m}{q_{m,\text{flat}}} (A_r^+)^{-1}$
 r = radial distance from axis of cylindrical fin
 Ra_D = Rayleigh number for a horizontal cylinder of diameter $D = \frac{g\beta_f(\Delta T)D^3}{\nu_f\alpha_f}$

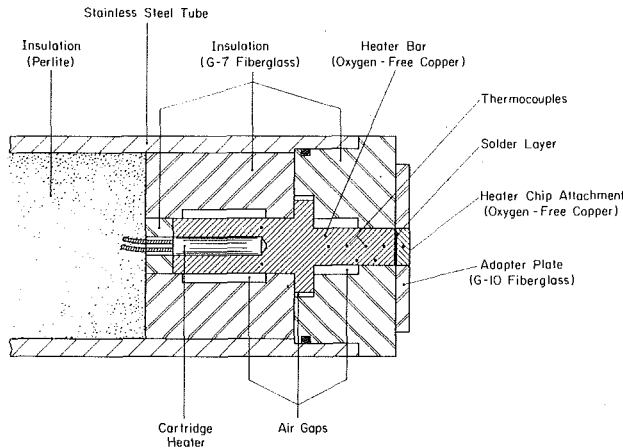


Fig. 2 Sectional diagram of the test heater

The light source provided the required luminosity during short flash durations, resulting in a 1/3000 second exposure time.

3 Numerical Results

Practical Design Considerations. The design of finned surfaces for electronic chips must satisfy several stringent requirements. Of paramount importance are: (1) increasing critical heat flux above the maximum expected chip heat flux, (2) maintaining chip temperature below an acceptable limit, (3) preventing the temperature excursion at incipient boiling commonly encountered with low contact angle fluids, and (4) limiting the accumulation of vapor on the chip surface in order to minimize the growth of a thick vapor bubble layer on multichip modules. Although extended surfaces can be expected to satisfy the requirement of increasing heat dissipation from the chip, the choice of a fin geometry may promote many adverse effects, making requirements (2), (3), and (4) hard to achieve. Thus, increasing heat dissipation by finning must be accompanied by such important design changes as subcooling the dielectric fluid or using a fluid with a boiling point much lower than the maximum acceptable chip temperature.

Preventing the incipience excursion leaves very few acceptable geometries for fin design. Anderson and Mudawar (1989) examined the feasibility of enhancing chip cooling performance by machining microstructures (rectangular microgrooves or

square microstuds) into the surface. They reported a significant reduction in wall superheat and CHF enhancement by factors as high as 2.51 over a smooth surface; yet, these attractive results were coupled with incipience temperature excursions as high as 14.3°C. Mudawar and Anderson (1990) attempted to reduce the incipience excursion on a vertically mounted chip by the high thermal mass of a tapered (pyramid-shaped) fin with microgrooves machined into its perimeter. Boiling was observed to commence near the base. The inclined downward facing side of the tapered fin allowed bubbles from the base to rapidly activate boiling on the entire surface, resulting in a noticeable excursion in the base temperature. Thus, they suggested that enhanced electronic cooling surfaces be designed to spread nucleation in a gradual manner with increasing heat flux. They concluded that chip extended surface geometries should be limited to horizontal, cylindrical shapes. The present study examines the cylindrical shape as a basic building block in the design of enhanced surfaces.

Numerical Results for Fin Effectiveness. Numerical heat conducting codes were used to predict the effectiveness of smooth horizontal cylindrical fins in saturated FC-72 and FC-87 having boiling points of 56°C and 30°C at one atmosphere, respectively. Fin effectiveness solutions were generated for a cylindrical fin in FC-72 enhanced circumferentially by either microgrooves or microstuds. Various fin materials were examined to evaluate the influence of thermal conductivity on fin effectiveness. Copper, aluminum and brass, having conductivities of 391, 240 and 110 W/m·K, respectively, were the reference materials for the numerical study.

The simulation of fin heat transfer during natural convection and nucleate boiling was simplified by assuming constant thermal conductivity, fluid temperature and base temperature, and by ignoring radiative heat transfer. The cylindrical fins were assumed to experience axisymmetric heat transfer according to the equation

$$\frac{\partial^2 T}{\partial x^2} + \frac{1}{r} \frac{\partial}{\partial r} \left(r \frac{\partial T}{\partial r} \right) = 0 \quad (1)$$

where x is the distance from the base measured along to the fin axis and r emanates radially from the axis.

The calculation domain was divided into a uniform grid of control volumes following the procedure suggested by Patankar (1980). Following Haley and Westwater (1966) and Nakayama et al. (1984), the local boiling heat transfer flux on the fin surface at a distance x from the base was assumed equal

Nomenclature (cont.)

Ra_l = Rayleigh number for a vertical plate of height
 $l = \frac{g\beta_f(\Delta T)l^3}{\nu_f\alpha_f}$
 $\Delta T = T_w - T_\infty$
 ΔT_h = wall temperature drop at incipience
 $\Delta T_i = T_{w,i} - T_\infty$ (or $T_{w,i} - T_{sat}$ for saturated boiling)
 ΔT_m = wall superheat at CHF
 ΔT_{sat} = wall superheat = $T_w - T_{sat}$
 ΔT_{sub} = bulk liquid subcooling = $T_{sat} - T_\infty$
 T_w = mean temperature at the base of enhanced surface attachment
 $T_{w,i}$ = incipient boiling temperature at the base of enhanced surface
 T_∞ = bulk liquid temperature

T_{85} = 85°C base temperature
 w = characteristic fin width and fin clearance of microgrooves and microstuds = 0.305 mm
 x = distance from the base of the cylindrical fin measured along axis
 α_f = thermal diffusivity of liquid
 β_f = expansion coefficient of liquid
 γ = bubble departure diameter scaling factor
 ϵ_e = effectiveness of finned element = $[Q_f + q_b(A_e - A_b)] / [q_b A_e]$
 ϵ_f = effectiveness of cylindrical fin = $\frac{Q_f}{q_b A_b}$
 ϵ_{chip} = overall effectiveness of enhanced surface

η_e = efficiency of finned element = $[Q_f + q_b(A_e - A_b)] / [q_b(A_f + A_e - A_b)]$
 η_f = efficiency of cylindrical fin = $\frac{Q_f}{q_b A_f}$
 λ_D = Taylor "most dangerous wavelength"
 $= 2\pi \left[\frac{3\sigma}{(\rho_f - \rho_g)g} \right]^{1/2}$
 λ_T = Taylor wavelength
 $= 2\pi \left[\frac{\sigma}{(\rho_f - \rho_g)g} \right]^{1/2}$
 ν_f = kinematic viscosity of liquid
 ρ_f = density of liquid
 ρ_g = density of vapor
 σ = surface tension

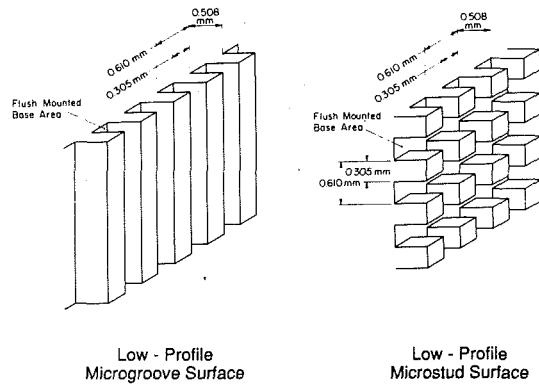


Fig. 3 Reference boiling curves used in the numerical effectiveness plots

to that of an isothermal surface at the same temperature regardless of surface orientation. The specific relationships between the heat flux and surface superheat were obtained from multi-segment linearized curve fits to data obtained for boiling on a flat vapor-blasted surface, and low-profile microgroove and microstud reference surfaces, Fig. 3, measured previously by the authors (Anderson and Mudawar, 1989). Since the incipience temperature excursion is surface specific, and practically nonexistent with extended cylindrical surfaces (as shall be demonstrated in the experimental results of the present study), the linearized boiling curves of the low-profile microgroove and microstud reference surfaces were adjusted in the incipience excursion region by a downward extrapolation of the linearized segment corresponding to nucleate boiling following incipience, to the point of intersection with the linearized fit to the natural convection data. Tables 1 and 2 give the power law coefficients for the linearized boiling curve data in the form

$$q = a(\Delta T_{\text{sat}})^n \quad (2)$$

where the power law coefficients a and n are valid only within the temperature range specified. The upper limits on wall su-

Table 1(a) Power law coefficients for the linearized smooth surface boiling curve (saturated FC-72)

Region	$q = a(\Delta T_{\text{sat}})^n$ $q(10^{-4} \text{ W/m}^2), \Delta T_{\text{sat}} (\text{°C})$		
	a	n	ΔT_{sat} range
I	0.070305	0.961112	0.0–6.9
II	0.0042862	2.409421	6.9–9.2
III	6.20582×10^{-6}	5.355373	9.2–13.6
IV	0.043817	1.959946	13.6–17.6
V	1.771535	0.669954	17.6–38.1

Table 1(b) Power law coefficients for linearized smooth surface boiling curve (saturated FC-87)

Region	$q = a(\Delta T_{\text{sat}})^n$ $q(10^{-4} \text{ W/m}^2), \Delta T_{\text{sat}} (\text{°C})$		
	a	n	ΔT_{sat} (°C)
I	0.069711	1.072335	0.0–3.9
II	0.016067	2.150660	3.9–6.5
III	6.577022	0.025611	6.5–11.4
IV	0.088282	1.796897	11.4–15.1
V	2.596540	0.551379	15.1–33.5

Table 2(a) Power law coefficients for linearized low-profile microgroove reference surface boiling curve (saturated FC-72)

Region	$q = a(\Delta T_{\text{sat}})^n$ $q(10^{-4} \text{ W/m}^2), \Delta T_{\text{sat}} (\text{°C})$		
	a	n	ΔT_{sat} range
I	0.066036	1.147633	0.0–5.1
II	1.874859×10^{-5}	6.166540	5.1–7.0
III	0.067283	1.960001	7.0–13.5
IV	0.181361	1.579018	13.5–21.0
V	5.080478	0.484374	21.0–35.3
VI	3.045850	0.627932	35.3–47.5

Table 2(b) Power law coefficients for linearized low-profile microstud reference surface boiling curve (saturated FC-72)

Region	$q = a(\Delta T_{\text{sat}})^n$ $q(10^{-4} \text{ W/m}^2), \Delta T_{\text{sat}} (\text{°C})$		
	a	n	ΔT_{sat} range
I	0.112661	1.074969	0.0–4.7
II	1.587379×10^{-4}	5.296950	4.7–6.2
III	6.226659×10^{-3}	3.285856	6.2–8.9
IV	0.216195	1.663139	8.9–15.8
V	4.761849	0.541072	15.8–30.2
VI	2.865880	0.690070	30.2–45.6

perheat values in Tables 1 and 2 correspond to the CHF point associated with the individual reference surface.

Natural convection is sensitive to both surface geometry and orientation. To systematically model natural convection, the non-boiling regions of the experimentally-determined, linearized boiling curves were replaced with appropriate information based on geometry-specific correlations. The natural convection heat transfer from the perimeter of the cylinder was calculated by the Churchill and Chu (1975a) correlation for a horizontal cylinder,

$$\overline{\text{Nu}}_D = \left\{ 0.60 + \frac{0.387 \text{ Ra}_D^{1/6}}{[1 + (0.559/\text{Pr}_f)^{9/16}]^{8/27}} \right\}^2 \quad (3)$$

The natural convection heat transfer coefficient for the circular tip was evaluated by dividing the tip area into thin vertical flat plates and integrating over the tip area. The heat transfer coefficient for each flat plate of length l was determined by Churchill and Chu's (1975b) correlation

$$\overline{\text{Nu}}_l = \left\{ 0.825 + \frac{0.387 \text{ Ra}_l^{1/6}}{[1 + (0.492/\text{Pr}_f)^{9/16}]^{8/27}} \right\}^2 \quad (4)$$

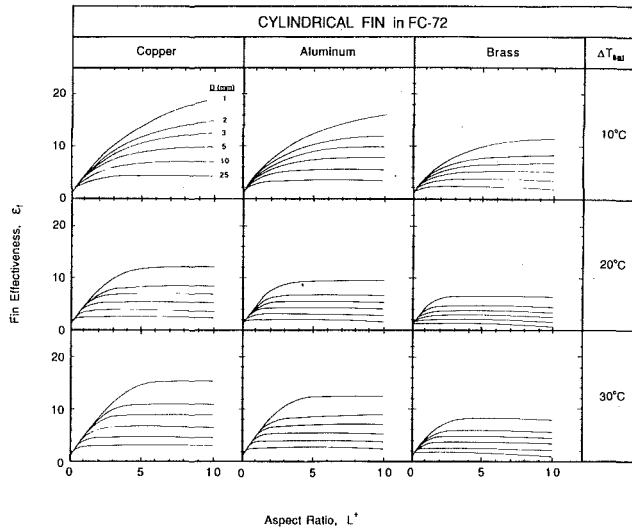


Fig. 4(a)

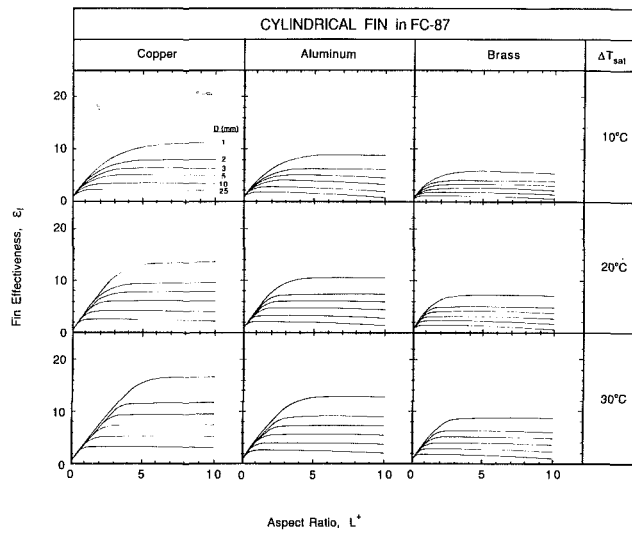


Fig. 4(b)

Fig. 4 Effectiveness plots for heat transfer from a horizontal smooth-surfaced cylindrical fin to (a) saturated FC-72 and (b) saturated FC-87

The numerical results are presented in Figs. 4 and 5 as plots of fin effectiveness, ϵ_f , versus aspect ratio, L^+ , for a given saturated fluid with fixed fin thermal conductivity and base superheat, ΔT_{sat} . The fin effectiveness is defined as the total heat transfer rate from the fin, Q_f , normalized by the heat transfer rate from the reference flat or low-profile microfinned surface, Fig. 3, having a planform area and temperature equal to those of the fin base.

$$\epsilon_f \equiv \frac{Q_f}{q_b A_b} \quad (5)$$

The experimentally determined values of q_b are given in Table 3 for several fluid/surface combinations and four values of base superheat. Fin efficiency, η_f , which represents a measure of the reduced performance due to conduction resistance within the fin is defined as

$$\eta_f \equiv \frac{Q_f}{q_b A_f} \quad (6)$$

where A_f is the total heat transfer area of the fin. Thus, effectiveness and efficiency are directly related by the ratio of total heat transfer area to base area,

$$\epsilon_f = A_f^+ \eta_f \quad (7)$$

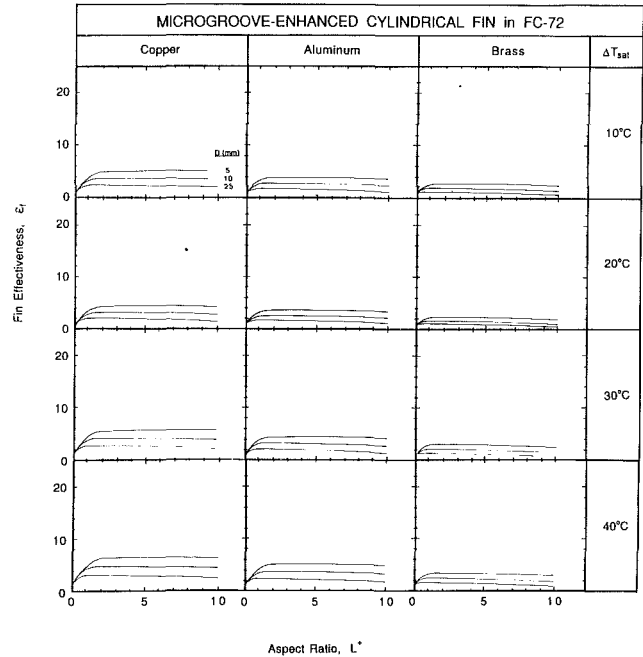


Fig. 5(a)

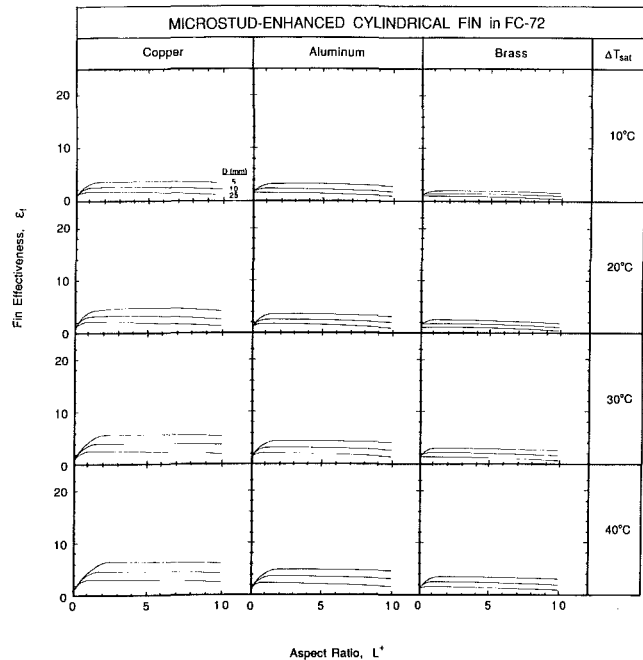


Fig. 5(b)

Fig. 5 Effectiveness plots for heat transfer to saturated FC-72 from a horizontal cylindrical fin with (a) microgroove and (b) microstud enhancement

For a given thermal conductivity and base superheat, Figs. 4 and 5 show effectiveness increases with aspect ratio to a peak value after which it remains constant or decreases. The maximum value of effectiveness is indicative of a trade-off between increased surface area and increased conduction resistance. Increasing fin diameter promotes peak effectiveness values at lower aspect ratios for a related reason. The tip of a large diameter fin comprises a large fraction of total fin heat transfer area and, therefore, conveys a large portion of the heat. This moves the peak effectiveness point toward lower aspect ratios compared with small diameter fins. Decreasing the thermal conductivity leads to decreased effectiveness for a fixed ge-

Table 3 Heat flux data for normalization of fin heat transfer rates

Heat flux of reference surface based on planform area, $q_b(10^{-4} \text{ W/m}^2)$	Base superheat $\Delta T_{\text{sat}} (\text{ }^\circ\text{C})$			
	10	20	30	40
	Flat reference surface (FC-72)	1.41	13.18	17.30
Flat reference surface (FC-87)	6.98	13.54	16.94	-
Low-profile microgroove reference surface (FC-72)	6.14	20.56	26.39	30.88
Low-profile microstud reference surface (FC-72)	9.95	24.08	29.99	36.54

ometry and may even result in effectiveness values below unity. This trend is clearly observed in Figs. 4 and 5 for large diameter fins with large aspect ratios. The high internal conduction resistances of these fins confine nucleate boiling to a very short distance from the base, leaving most of the fin surface undergoing natural convection, a condition less favorable than a bare surface undergoing boiling. Figures 4 and 5 demonstrate that, for a specific fin material at high base temperature, the effectiveness curves for various diameters initially follow a common path, while at low base superheat the curves diverge at relatively low aspect ratios.

Elemental Approach to Determining Enhanced Surface Performance. An elemental approach was employed in the calculation of effectiveness for the enhanced surfaces. Elements of surface area, A_e , were defined as identical sections of the flat surface of a chip to which a cylindrical (pin) fin is attached. Superposition of the heat transfer rate from a fin and the surrounding bare surface of an element was based on the assumption that the heat flux/wall superheat characteristics of the bare surface are insensitive to the presence of the fin. The primary advantage of this elemental approach is the ease of extension to computing the effectiveness of an entire chip covered with multiple fins. The surface was assumed to be covered with elements of identical effectiveness. One obvious limitation to this assumption is the complexity of natural convection over multi-finned surfaces and the lack of uniformity in the convection coefficient between the various elements. However, numerical results demonstrate that variations in the magnitude of the natural convection coefficient have a weak influence on the heat transfer rate from fins undergoing mostly nucleate boiling. Another limitation of the elemental analysis is the potential thickening of a vapor bubble layer on multi-finned surfaces. This problem is addressed in detail in conjunction with the experimental results of this study.

Knowing the effectiveness of the fin itself, the effectiveness and efficiency of a finned element of area A_e can be determined from the relations

$$\epsilon_e = 1 + \frac{\epsilon_f - 1}{A_e^+} \quad (8)$$

$$\eta_e = \frac{1}{A_f^+ + A_e^+ - 1} + \frac{1}{1 + \frac{A_f^+}{A_e^+ - 1}} \quad (9)$$

where $A_e^+ = A_e/A_b$.

For chips covered with m identical elements, the overall chip effectiveness is determined by the area-weighted average

$$\epsilon_{\text{chip}} = \frac{1}{A_{\text{chip}}} \sum_{i=1}^m \epsilon_e, \quad iA_e, \quad i = \epsilon_e \quad (10)$$

The proper layout and sizing of elements on a chip surface

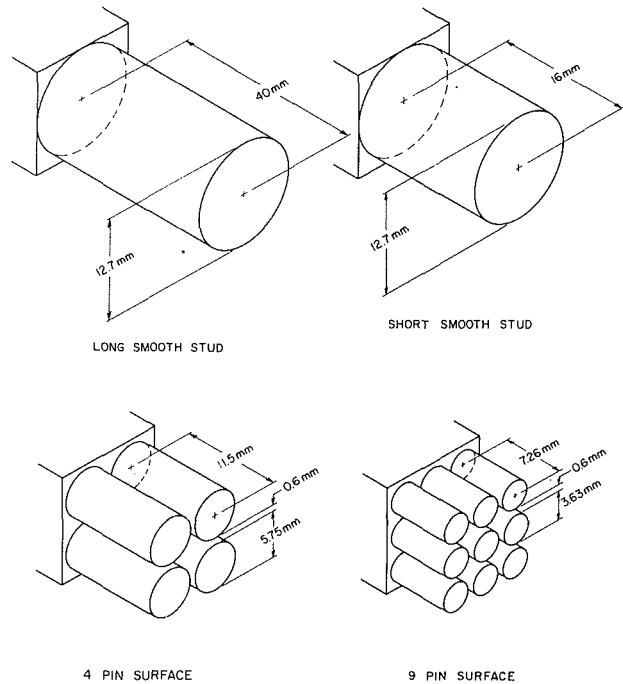


Fig. 6 Geometries of smooth studs and pin fin arrays

is limited by the possibility of severe vapor coalescence and accumulation between the fins, which may promote the formation of a vapor blanket and result in CHF. Because the critical spacing between fins is related to the generation of vapor bubbles, it is proposed that the spacing be related to the bubble departure diameter, D_b , by a scaling factor γ . Bondurant and Westwater (1971) tested radially finned horizontal tubes boiling in R-113 and found that the critical clearance between fins was in the range of the nucleate boiling departure diameter. Further experiments by Klein and Westwater (1971) using a nine pin array confirmed that a bubble departure diameter was the optimal spacing for fin arrays. Based on these findings, the scaling factor, γ , was set equal to one for the design of enhanced boiling surfaces used in the present study. Photographs obtained in the present study indicated the average D_b value for saturated boiling of FC-72 and FC-87 was approximately 0.61 mm. Accordingly, the diameter of pin fins arranged in an $m \times m$ array on a square chip of length L_{chip} was determined as

$$D = \frac{L_{\text{chip}} - mD_b}{m} \quad (11)$$

4 Experimental Results

The numerical codes used to generate the effectiveness plots were modified to output boiling curves based on the geometries of several enhanced surface structures used in the experimental study. The numerical predictions estimate boiling performance up to the CHF point corresponding to the flat, microgroove or microstud reference surfaces. The generalized nature of the numerical scheme allows much flexibility in the specification of design envelope. For the present study, various metallic attachments were designed to enhance heat transfer from a $12.7 \times 12.7 \text{ mm}^2$ simulated microelectronic heat source.

4.1 Pin-Fin Surface Geometries. The experimental enhancement surfaces were based on cylindrical shapes fabricated from high purity copper and arranged either as single studs or in pin arrays. Each of the enhanced surfaces was vapor blasted with an air/water/silica slurry to ensure uniform surface characteristics (Anderson and Mudawar, 1989). The two smooth stud enhanced surfaces, Fig. 6, differed only in length. The

Table 4 Ratio of total heat transfer area to planform base area for the enhanced surfaces of the present study

Enhanced surface Geometry	Total heat transfer surface area ^(a) A_t (cm ²)	Area ratio ^(b) $A_t^+ = \frac{A_t}{A_{chip}}$
Flat (reference)	1.61	1.00
Low profile microgroove (reference)	3.54	2.26
Low profile microstud (reference)	3.85	2.39
Short smooth stud	8.00	4.96
Long smooth stud	17.57	10.89
4 pin	9.92	6.15
9 pin	9.06	5.62
Axial microgroove stud	11.21	6.95
Radial microgroove stud	12.34	7.65
Microstud stud	14.74	9.14

^(a)Planform area of chip $A_{chip} = 1.61$ cm².

^(b) A_t included the heat transfer area of the extended surface plus the unfinned chip base area.

16 mm “short” smooth stud conformed to typical packaging limitations, while the 40 mm long smooth stud was tested for photographic analysis of the interactions of multiple modes of heat transfer on a horizontal cylinder.

The 4-pin and 9-pin surfaces, Fig. 6, provided information on the performances of pin fin arrays. The spacing between the pins was set at one bubble departure diameter and the length-to-diameter aspect ratio was set at 2 to enforce practical spatial packaging requirements of multichip modules. The 4 and 9-pin structures were fabricated from a single bar of oxygen-free copper by electric-discharge machining (EDM) to alleviate the contact resistance that accompanies soldered assembly. Table 4 details the actual heat transfer areas and the ratios of total surface to chip base areas for each of the enhanced chip attachments.

The enhancement of boiling by extended surfaces can be measured in different forms as discussed in the previous section. To a packaging engineer charged with dissipating the maximum possible heat rate from an electronic device of fixed dimensions while maintaining the desired device temperature, the most meaningful measure of heat flux is total heat transfer rate divided by the surface area of the device; heat flux based on the total wetted area of the enhanced surface attachment is of little importance in this situation provided the enhancement meets the volumetric constraints in the packaging of multi-module electronic hardware. For this reason, unless specified otherwise, the boiling curves presented hereafter have been based on heat dissipation rate per unit chip planform area, 12.7×12.7 mm², and mean temperature at the base of the enhanced surface attachment, T_w .

Flow Visualization of Boiling on Pin-Fin Surfaces. Several experiments were performed with the long, smooth stud to photograph the evolution of boiling pattern with increased heat flux. Figure 7 shows side and end views of the stud in saturated FC-87. One distinct feature of boiling behavior at heat fluxes slightly above incipience is the concentration of active nucleation sites near the upper side of the stud. This observation illustrates one weakness with axisymmetric numerical models for boiling on cylindrical fins. As heat flux was increased, the nucleation front advanced toward the tip with more circumferential boiling uniformity except for a narrow region close to the nucleation front. Close-up end-view examination of the surface showed the bubbles emanating normal to the stud surface with a uniform bubble departure diameter independent of circumferential location. However, this phenomenon was visually obscured by the buoyancy forces pulling the bubbles toward the upper surface of the stud. As heat flux was increased to only 27 percent of CHF, nucleation covered the entire perimeter except for the tip, which was partially undergoing natural convection in liquid. Boiling near the base of the stud

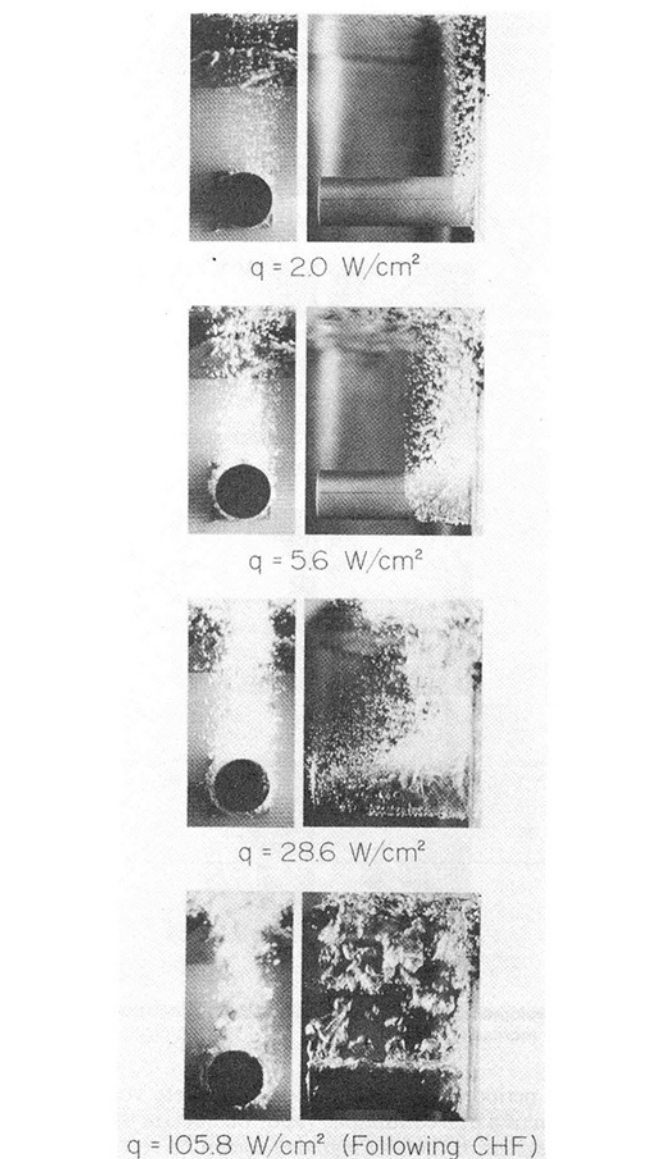


Fig. 7 Development of boiling pattern on the long smooth stud in saturated FC-87 with increasing heat flux

was very vigorous and bubble coalescence into large vapor jets and columns was very noticeable. Isolated nucleate boiling was confined to regions near to or on the tip. Transition to film boiling occurred at $q_m = 105.8$ W/cm². The stud tip and perimeter were fully encased in a fairly smooth vapor layer which accumulated vapor at the upper surface of stud. The vapor was released from the crests of five vapor waves having a mean wavelength of 8.0 mm compared to a predicted Taylor’s “most dangerous wavelength” in FC-87 of $\lambda_D = 7.87$ mm.

Figure 8 shows side and end views of boiling on the 4-pin surface in saturated FC-87. As in the case of boiling from a single cylindrical stud, nucleation was initiated near the base of the pins. At fluxes slightly above incipience, the nucleation front moved toward the pin tips, totally engulfing the upper pins, while the lower pins were partially undergoing natural convection. However, a slight increase in heat flux to approximately 6 percent of CHF activated nucleation over the entire surface. This would indicate that numerical models of boiling heat transfer from a pin fin array based on identical heat transfer performances of individual pins would be less successful for heat fluxes close to incipience. When the heat flux was increased to the CHF value of 89.8 W/cm², a single continuous vapor blanket engulfed the enhanced surface, al-

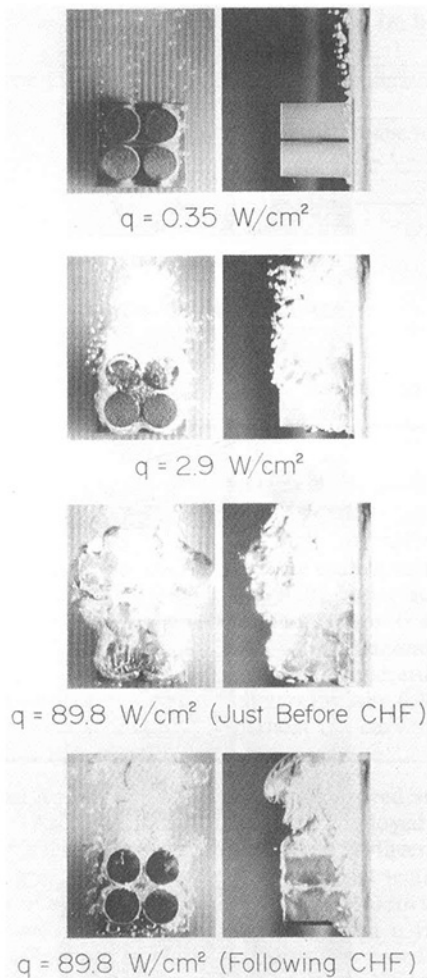


Fig. 8 Development of boiling pattern on the 4-pin surface in saturated FC-87 with increasing heat flux

lowing a periodic release of vapor in discrete volumes. The formation of a thin continuous vapor blanket on the perimeter and tip regions of the pins signaled transition to film boiling.

Saturated Boiling on Pin-Fin Surfaces. Figure 9 shows FC-87 boiling data for the long and short smooth studs displayed in Fig. 6. The slope of the natural convection line is greater than the predicted slope for a horizontal cylinder. End effects caused by the presence of the heat source module at the stud base may account for this discrepancy. In the nucleate boiling region the numerical solution fits the experimental data closely. This result lends credibility to the modeling assumption that localized boiling heat transfer from a non-isothermal surface is similar to that from an isothermal surface at the same temperature regardless of surface orientation. However, it should be emphasized that the numerical study was not specifically aimed at predicting CHF since the hydrodynamic conditions associated with CHF on a cylinder differ markedly from those on a vertical flat surface. Although the upper heat flux limit for the numerically-determined boiling curve corresponds to local enhanced surface conditions identical to those of a flat surface at CHF, the upper limit should merely be treated as signaling a tendency of the surface to promote local vapor blanketing.

Although the long stud had over twice the surface area of the short stud, Fig. 9 shows CHF for the long stud was only 30 percent higher. Based on photographic analysis of the boiling stud, it can be concluded that the modest enhancement is a result of local dryout near the base of the fin. As the base heat flux and superheat rose to a point great enough to sustain

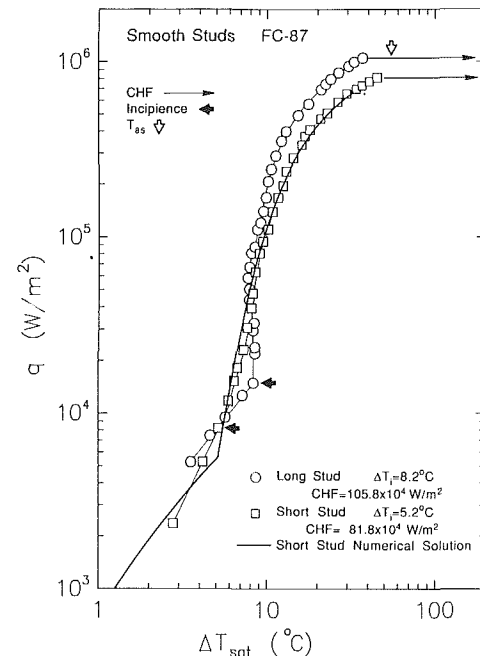


Fig. 9 Boiling curves for the long and short smooth studs in saturated FC-87

a small but stable vapor blanket, the insulating effect of the blanket introduced additional conduction resistance between the fin base and the now decreased nucleate boiling heat transfer area. Thus, the base superheat increased in response to the combined effects of increased internal conduction resistance and decreased heat transfer area. Further increase in base heat flux pushed the fin heat transfer equilibrium toward a condition where the vapor blanket area increased unrestrained and caused CHF.

The validity of superposition of cylindrical fin elements was tested using the 4 and 9-pin surfaces shown in Fig. 6. Experimental data in the nucleate boiling region for the 4-pin surface, Fig. 10(a), are closely predicted by the numerical model based on superposition of four identical elements, each carrying a smooth stud. The 9-pin surface, Fig. 10(b), apparently experienced more pin-to-pin interference than the 4-pin array since the 9-pin data is shifted by approximately 2.5°C to the left of the predicted curve. Nevertheless, the agreement is still acceptable for electronic packaging purposes.

4.2 Multi-Level Surface Enhancement. The surface enhancement results of the pin-fin surfaces reported in this paper as well as those of the low-profile microgroove and microstud surfaces and of other flat, textured surfaces (Anderson and Mudawar, 1989) all point to the potential for significant enhancement of boiling performance which can result from combining the various augmentation geometries into a single chip surface attachment. Figure 11 shows three surface attachments whose geometries were based upon three levels of enhancement: (1) a single extended cylindrical stud, (2) low profile microstructures machined into the stud perimeter, and (3) microscopic surface characteristics achieved by blasting the surface with an air/water/silica slurry prior to testing. The axial and radial microgroove enhanced studs were constructed by grooving a smooth stud along the axial and radial directions, respectively. The microstud-enhanced stud consisted of a microstud geometry machined into the smooth stud. The surface microstructures shown in Fig. 11 are identical to those of the low-profile reference surfaces (see Fig. 3). Figure 11 also shows various length scales associated with the microstructured stud attachments. The microscopic characteristics resulting from vapor blasting influence the incipience and low nucleation den-

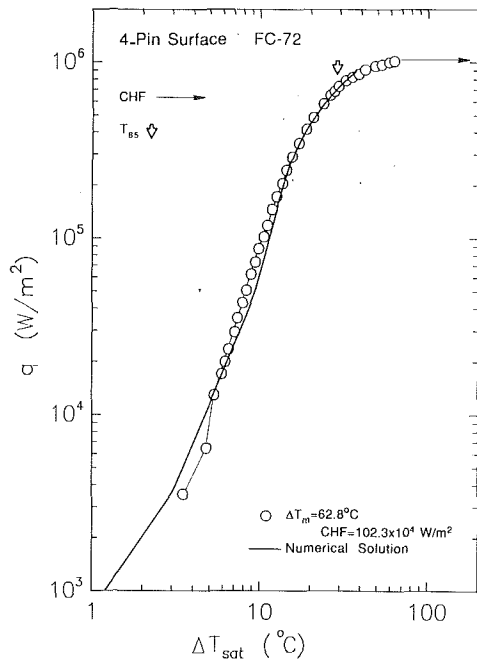


Fig. 10(a)

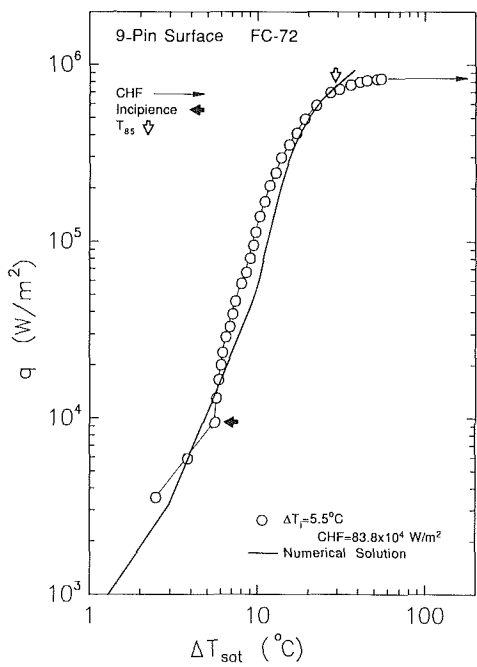
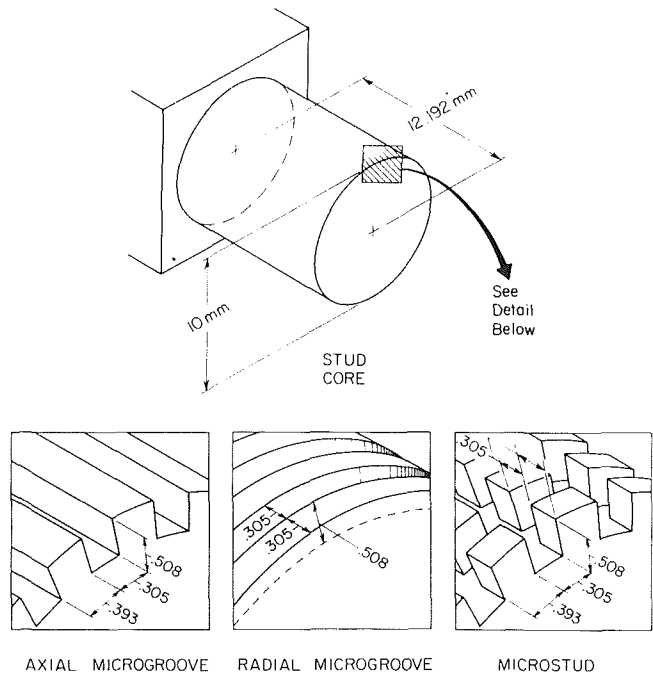


Fig. 10(b)

Fig. 10 Boiling curves for the (a) 4-pin and (b) 9-pin surfaces in saturated FC-72

sity regions of the boiling curve (Anderson and Mudawar, 1989). The machined microstructures, on the other hand, act as active nucleation sites during more developed boiling since the characteristic fin and gap widths for these microstructures are smaller than a typical bubble departure diameter. The diameter of the studs was roughly two times greater than the Taylor wavelength, λ_T (5.87 mm for FC-72) and approximately equal to the Taylor "most dangerous" wavelength $\lambda_D (= \sqrt{3}\lambda_T)$ associated with CHF. Therefore, it was expected that CHF would be accompanied by the formation of a single vapor blanket in the cross-wise plane of these fins.

Data for the microgroove-enhanced surfaces in saturated FC-72 are shown in Fig. 12(a). In the natural convection region,



AXIAL MICROGROOVE RADIAL MICROGROOVE MICROSTUD

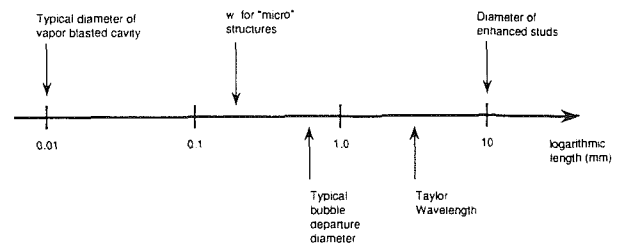


Fig. 11 Geometries of the enhanced stud surface and associated characteristic length scales

the axially-grooved stud turbulated the induced liquid flow more effectively than the radially-grooved stud as evidenced by the higher natural convection heat transfer rate for the axially-grooved stud. Numerically, the distinction between the direction of the grooves is not taken into consideration; hence, the predicted boiling curves are equivalent for both structures, based on the low-profile microgroove data provided in Fig. 3 and Table 2(a). Figure 12(b) shows a slight discrepancy between numerical predictions and experimental data for the microstud-enhanced stud based on the reference low-profile microstud data given in Fig. 3 and Table 2(b), especially in the low heat flux region. This surface achieved a CHF value of 105.4 W/cm² in saturated FC-72, the highest of all the enhanced surface geometries.

Experiments were performed to combine the attractive features of subcooled boiling with the high CHF values of the enhanced-stud surfaces. Comparisons of saturated and subcooled boiling curves for the low profile microstud reference surface, Fig. 3, and microstud-enhanced stud, Fig. 11, are shown in Figs. 13(a) and 13(b), respectively. Figure 13(a) shows how subcooling eliminated the incipience excursion associated with saturated boiling on the reference microstud surface and increased CHF by 42 percent. The numerical results for subcooled boiling show good agreement with the microstud-enhanced stud, Fig. 13(b), like it did for saturated boiling. The same surface produced the highest heat flux in the present study with subcooled boiling. The 159.3 W/cm² heat dissipation capability of this surface suggests pool boiling is a viable alternative for cooling even very high power electronic chips.

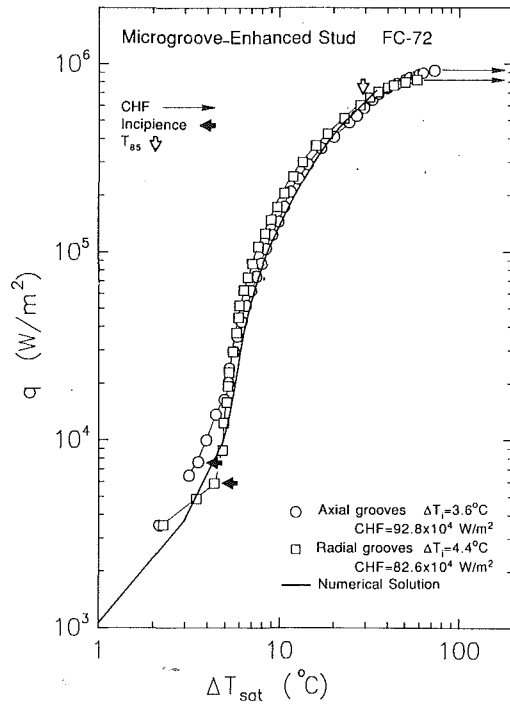


Fig. 12(a)

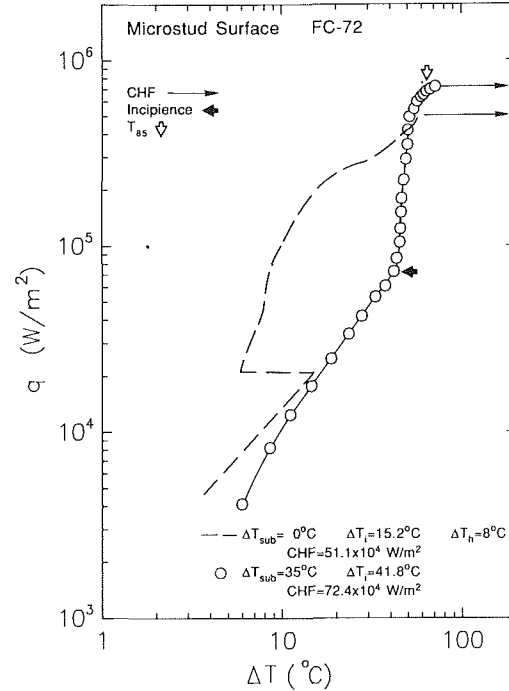


Fig. 13(a)

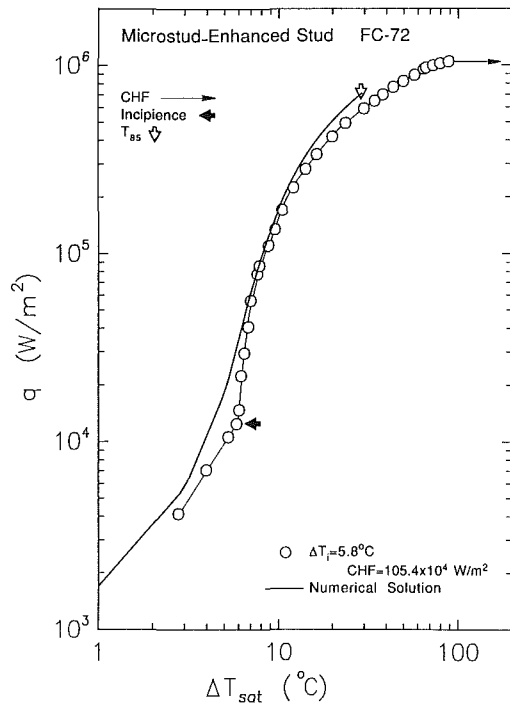


Fig. 12(b)

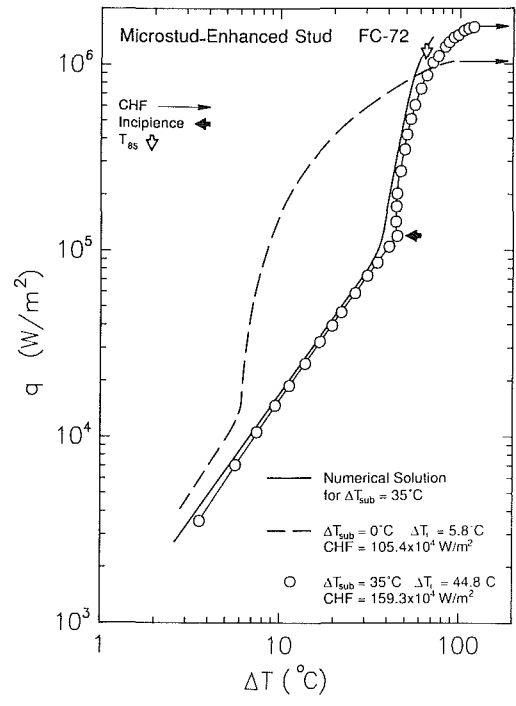


Fig. 13(b)

Fig. 12 Boiling curves for the (a) axially and radially grooved enhanced stud and (b) microstud-enhanced stud in saturated FC-72

Fig. 13 Effect of subcooling on the boiling curves for (a) the low-profile microstud reference surface and (b) microstud-enhanced stud in FC-72

Figure 14 shows a comparison of boiling behavior from the microstud-enhanced stud in saturated FC-72 and 35°C subcooled FC-72. Saturated boiling followed the general trend of boiling from a horizontal cylindrical surface. Nucleation commenced near the base with bubble departure diameters greater than the 0.305 mm microstud gap. Full activation of nucleate boiling over the entire perimeter and portions of the tip occurred at only 10.4 percent of CHF. Fully-developed boiling with severe vapor effusion was observed at approximately 46.5 percent of CHF. Following CHF, a thin vapor film formed

on the perimeter and tip regions, and vapor was released at the upper surface of the stud from one or two jets. Subcooled tests, Fig. 14, showed very noticeable differences in boiling behavior compared with saturated boiling. First, the bubbles were much smaller and emerged from within the microstud gaps. Second, most of the bubbles condensed in the subcooled pool just after departing the enhanced surface. Even during fully-developed boiling ($q = 28.6 \text{ W/cm}^2$), the large mass of vapor was almost totally condensed over a vertical distance equivalent to the stud diameter. Condensation at the vapor-

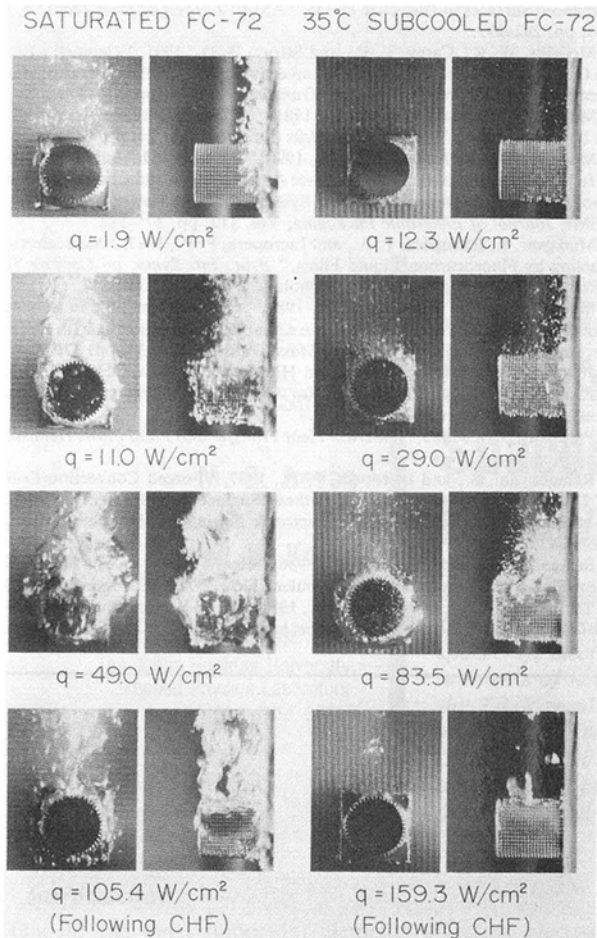


Fig. 14 Comparison of the development of boiling pattern on the microstud-enhanced stud in saturated and subcooled FC-72

liquid interface of the vapor layer surrounding the enhanced surface during film boiling also reduced the amount of vapor considerably, and vapor was released from the stud in relatively small bubbles which diminished in size following departure into the subcooled liquid.

Very important practical conclusions may be drawn from these subcooled boiling experiments. First, subcooling significantly enhances boiling performance and increases CHF. Subcooling may be essential in controlling bubble boundary layer growth on high power multichip modules.

4.3 CHF Results. Figure 15 shows a compilation of CHF data normalized with respect to CHF for a vertical flat surface (20.3 W/cm^2) for all the surfaces examined in the present study. Each surface is represented by its value of A_r^+ , the ratio of total surface area to planform base area provided in Table 4.

The dimensionless CHF shown in Fig. 15 is a measure of "CHF fin efficiency" since

$$q_m^+ = \frac{q_m A_{\text{chip}}}{q_{m, \text{flat}} A_r} = \frac{q_m}{q_{m, \text{flat}}} (A_r^+)^{-1} \quad (12)$$

The normalized CHF value $q_m^+ = 1$ corresponds to surfaces whose CHF enhancement over a flat surface is balanced by the increased conduction resistance within the extended surface. The conduction resistance raises the base temperature, promoting the formation of a localized vapor blanket in that region. Only the flat microstud surface effectively delayed CHF since it increased surface area considerably with only a mild increase in fin volume compared with the pin fin and enhanced stud surfaces.

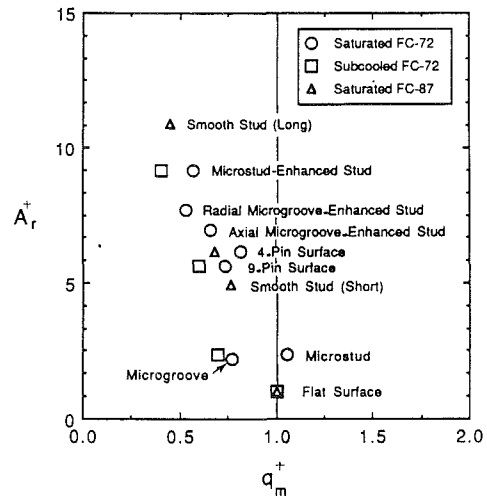


Fig. 15 CHF fin effectiveness for all the enhanced surfaces of the present study

Summary

The present study involved an examination of several surface geometries for the purpose of enhancing heat transfer from high power electronic chips. Specific results from the study are as follows:

1. The heat transfer performances of horizontal boiling cylindrical fins can be successfully predicted using two-dimensional axisymmetric heat diffusion models. The assumption that localized boiling heat transfer from an extended surface is similar to that from an isothermal surface at the same temperature, regardless of surface orientation, was proven effective in predicting boiling performance, except for low post-inception heat fluxes.

2. The elemental analysis based on extending single fin numerical results to fin arrays was successful in predicting boiling curves for 4-pin and 9-pin enhanced surfaces. This approach constitutes a practical tool in the design of enhanced surfaces for multichip modules.

3. Combining different levels of enhancement is an effective means of improving chip heat dissipation rate. An optimum enhanced surface was constructed from a single extended cylindrical stud with microstructures machined into the stud perimeter, followed by blasting the surface with an air/water/silica slurry.

4. Subcooling is very effective in enhancing boiling performance and increasing CHF. Subcooling may be necessary for controlling bubble boundary layer growth on high power multichip modules.

5. The combined use of extended surfaces and subcooling is a viable alternative for cooling very high power electronic chips. Microstructured extended surfaces resulted in chip heat fluxes (based on planform area) of 105.4 and 159.3 W/cm^2 in saturated and 35°C subcooled FC-72, respectively.

Acknowledgment

Support for this research by the IBM corporation is gratefully acknowledged. The authors also appreciate receiving FC-72 and FC-87 fluid samples from the Industrial Chemical Products Division of 3M.

References

- Anderson, T. M., and Mudawar, I., 1989, "Microelectronic Cooling by Enhanced Pool Boiling of a Dielectric Fluorocarbon Liquid," *ASME Journal of Heat Transfer*, Vol. 11, pp. 752-759.
- Bondurant, D. L., and Westwater, J. W., 1971, "Performance of Transverse

Fins for Boiling Heat Transfer," *Chem. Eng. Prog. Symp. Series*, Vol. 113, pp. 30-37.

Cash, D. R., Klein, G. J., and Westwater, J. W., 1971, "Approximate Optimum Fin Design for Boiling Heat Transfer," *ASME Journal of Heat Transfer*, Vol. 93, pp. 19-24.

Churchill, S. W., and Chu, H. H. S., 1975a, "Correlating Equations for Laminar and Turbulent Free Convection from a Horizontal Cylinder," *Int. J. Heat Mass Transfer*, Vol. 18, pp. 1049-1053.

Churchill, S. W., and Chu, H. H. S., 1975b, "Correlating Equations for Laminar and Turbulent Free Convection from a Vertical Plate," *Int. J. Heat Mass Transfer*, Vol. 18, pp. 1323-1329.

Cumo, M., Lopez, S., and Pinchera, G. C., 1966, "Numerical Calculations of Extended Surface Efficiency," *Chem. Eng. Prog. Symp. Series*, Vol. 59, pp. 225-233.

Danielson, R. D., Krajewski, N., and Brost, J., 1986, "Cooling of a Superfast Computer," *Electronic Packaging and Production*, Vol. 26, pp. 44-45.

Grimley, T. G., Mudawar, I., and Incropera, F. P., 1988, "Limits to Critical Heat Flux Enhancement in a Liquid Film Falling over a Structured Surface which Simulates a Microelectronic Chip," *ASME Journal of Heat Transfer*, Vol. 110, pp. 535-538.

Haley, K. W., and Westwater, J. W., 1966, "Boiling Heat Transfer from Single Fins," *Proceedings 3rd International Heat Transfer Conference*, Chicago, Illinois, Vol. 3, pp. 245-258.

Klein, G. J., and Westwater, J. W., 1971, "Heat Transfer from Multiple Spines to Boiling Liquids," *AIChE J.*, Vol. 17, pp. 1050-1056.

Maddox, D. E., and Mudawar, I., 1989, "Single and Two-Phase Convective Heat Transfer from Smooth and Enhanced Microelectronic Heat Sources in a Rectangular Channel," *ASME Journal of Heat Transfer*, Vol. 111, pp. 1045-1052.

Marto, P. J., and Lepere, V. J., 1982, "Pool Boiling Heat Transfer from

Enhanced Surfaces to Dielectric Fluids," *ASME Journal of Heat Transfer*, Vol. 104, pp. 292-299.

McGillis, W. R., Carey, V. P., and Strom, B. D., 1991, "Geometry Effects on Critical Heat Flux for Subcooled Convective Boiling from an Array of Heated Elements," *ASME Journal of Heat Transfer*, Vol. 113, pp. 463-471.

Messina, A. D., and Park, E. L., 1981, "Effects of Precise Arrays of Pits on Nucleate Boiling," *Int. J. Heat Mass Transfer*, Vol. 24, pp. 141-145.

Mudawar, I., and Anderson, T. M., 1990, "Parametric Investigation into the Effects of Pressure, Subcooling, Surface Augmentation and Choice Coolant on Pool Boiling in the Design of Cooling Systems for High Power Density Chips," *ASME Journal of Electronic Packaging*, Vol. 112, pp. 375-382.

Mudawar, I., Incropera, T. A., and Incropera, F. P., 1987, "Microelectronic Cooling by Fluorocarbon Liquid Films," *Proc. Int. Symp. on Cooling Technology for Electronic Equipment*, Honolulu, March, pp. 340-357.

Mudawar, I., and Maddox, D. E., 1989, "Critical Heat Flux in Subcooled Flow Boiling of Fluorocarbon Liquid on a Simulated Electronic Chip in a Vertical Rectangular Channel," *Int. J. Heat Mass Transfer*, Vol. 32, pp. 379-394.

Nakayama, W., Nakajima, T., and Hirasawa, S., 1984, "Heat Sink Studs Having Enhanced Boiling Surfaces for Cooling of Microelectronic Components," *ASME Paper 84-WA/HT-89*.

Patankar, S. V., 1980, *Numerical Heat Transfer and Fluid Flow*, Hemisphere Publishing Corp., New York.

Ramadhani, S., and Incropera, F. P., 1987, "Forced Convection Cooling of Discrete Heat Sources with and without Surface Enhancement," *Proc. Int. Symp. on Cooling Technology for Electronic Equipment*, Honolulu, Mar., pp. 249-264.

Samant, K. R., and Simon, T. W., 1986, "Heat Transfer from a Small, High-Heat-Flux Patch to a Subcooled Turbulent Flow," *ASME Paper 86-HT-22*.

Tuckerman, D. B., and Pease, R. F., 1981, "High-Performance Heat Sinking for VLSI," *IEEE Electronic Device Letters*, Vol. 2, pp. 126-129.